

- for the largest tyrannosaur (138 cm and 120 cm; total, 258 cm). Skull length may thus be proportionately greater in carcharodontosaurids than in tyrannosaurids, which appear to have longer distal hind limb segments.
28. Diagnostic features for *C. saharicus*. **Dental:** Posterior crown margin only slightly concave at mid-length and convex distally; enamel ornamentation, including transverse bands and arcuate wrinkles near crown margins. **Cranial:** Antorbital fenestra length 30%, and height 25%, of those of the cranium; ventral margin of antorbital fossa everted; prefrontal absent or co-ossified; postorbital ventral ramus with robust lateral process with groove and pit; postorbital-squamosal articulation helical; and paroccipital processes and basal tubera positioned far ventral to occipital condyle. **Postcranial:** Postaxial cervical vertebrae with kidney-shaped posterior articular faces, short neural spines, robust transverse processes, and strong ventral keels; anterior caudal vertebrae with pleurocoels; and distal caudal vertebrae with narrow anteroposteriorly compressed neural spines.
29. Stromer's skeleton 1922 X46 provides an association between cranial and postcranial bones, including an exceptionally broad cervical vertebra and a pleurocoelous anterior caudal vertebra (4). These vertebrae, in turn, overlap with skeleton 1922 X45 (Stromer's "*Spinosaurus B*"), which provides additional information about the vertebral column and pedal phalanges (5).
30. J. W. Stovall and W. Langston Jr., *Am. Midl. Nat.* **43**, 696 (1950).
31. R. A. Coria and L. Salgado, *Nature* **377**, 224 (1995).
32. The holotypic specimen of *B. ingens* comprises two dorsal vertebrae, a neural arch, three sacral vertebrae, a rib fragment, pubes, and the proximal portion of the ischium (1922 X47) (5). Unlike the Moroccan skeleton, the shaft of the pubis is broader, the pubic foot is divided in the midline, and the iliac peduncle of the ischium is proportionately narrower.
33. **Etymology:** *Delta*, delta (Greek); *dromeus*, runner (Greek); *agilis*, quick (Latin). Named for the deltaic facies in which it was found and for the cursorial proportions of its hind limbs. The holotypic skeleton (SGM-Din 2) is in the collections of the Ministère de l'Energie et des Mines, Rabat, Morocco. **Diagnosis:** Anterior caudal vertebrae with broad quadrangular neural spines; coracoid and acromion broadly expanded anteroposteriorly; coracoid with shallow notch in anterior margin; ischial midshaft dorsoventrally compressed; femur with accessory trochanter on distal shaft; femoral medial distal condyle with anterior extension; metatarsal IV distal condyles reduced. **Referred material** (existing as figures only): Left coracoid, pubes, right femur, proximal right tibia, and left fibula (1912 VIII) (5). Femoral length (122 cm) is 1.5 times that of SGM-Din 2, indicating that *D. agilis* grew to an adult body size within the range established for *T. rex* (40).
34. H. F. Osborn, *Bull. Am. Mus. Nat. Hist.* **35**, 733 (1916).
35. J. F. Bonaparte and Z. Kielan-Jaworowska in *Fourth Symposium on Mesozoic Terrestrial Ecosystems, Short Papers*, P. J. Currie and E. H. Koster, Eds. (Occasional Paper 3, Royal Tyrrell Museum of Palaeontology, Drumheller, Alberta, Canada, 1987), pp. 24–29.
36. R. Molnar, *Mem. Soc. Geol. Fr.* **139**, 131 (1980); E. Buffetaut and J.-C. Rage, in *The Africa–South America Connection*, W. George and R. Lavocat, Eds. (Clarendon, Oxford, 1993), pp. 87–99.
37. J. F. Bonaparte, *Mus. Argent. Cienc. Nat. Paleontol.* **4**, 16 (1991); O. W. M. Rauhut and C. Werner, *Palaeontol. Z.* **69**, 475 (1995).
38. J. Calvo and L. Salgado, *Gaia*, in press.
39. J. I. Kirkland and D. Burge, *J. Vertebr. Paleontol.* **14**, 32A (1994).
40. P. L. Larson, *Paleontol. Soc. Spec. Pub.* **7**, 139 (1995).
41. A. G. Smith, D. G. Smith, B. M. Funnell, *Atlas of Mesozoic and Cenozoic Coastlines* (Cambridge Univ. Press, Cambridge, 1994), p. 38.
42. D. L. Swofford, PAUP 3.1 (Illinois Natural History Survey, Champaign, IL, 1993).
43. W. B. Harland et al., *A Geologic Time Scale 1989* (Cambridge Univ. Press, Cambridge, 1990).
44. C. W. Gilmore, *Bull. U.S. Nat. Mus.* **110**, 1 (1920).
45. The following 63 synapomorphies correspond with scored character states (Table 2) that were used in the analysis of basal tetanuran relationships presented in Fig. 4. **Tetanurae:** 1, maxillary fenestra; 2, lacrimal pneumatic excavation; 3, slot in ventral process of lacrimal for jugal; 4, jugal pneumatic excavation; 5, prefrontal-frontal peg-in-socket articulation; 6, posteriormost maxillary tooth positioned anterior to orbit; 7, axial neural spine broadened distally; 8, chevron bases with paired anterior and posterior processes; 9, semilunate carpal with transverse trochlea; 10, manual digit III reduced (metacarpal III shaft diameter is 50% or less that of metacarpal II); 11, iliac-ischial articulation smaller than iliac-pubic articulation; 12, ischial obturator notch; 13, femoral anterior trochanter blade-shaped; 14, tibial distal end backing calcaneum; 15, fibular distal end reduced (less than twice anteroposterior width at mid-shaft); 16, astragalar ascending process plate-shaped (state 1); 17, astragalar cup for fibula reduced; 18, astragalar distal condyles oriented anteroventrally; 19, astragalar condyle with anterior groove; 20, metatarsal III with hourglass-shaped proximal end; 21, metatarsal III with wedge-shaped midshaft. **Neotetanurae:** 22, promaxillary recess extends into maxillary anterior ramus; 23, ectopterygoid pneumatic excavation invaginated laterally; 24, splenial with notched anterior margin of internal mandibular fenestra; 25, retroarticular surface of articular facing posteriorly; 26, posterior chevrons L-shaped; 27, furcula (fused clavicles); 28, coracoid posterior process and fossa crescent-shaped; 29, iliac preacetabular fossa present; 30, iliac pubic peduncle twice as long anteroposteriorly as broad transversely; 31, pedal digit I-phalanges 1 + 2 subequal in length to pedal digit III-phalanx 1. **Spinosauroidea** (plus included node): 32, anterior ramus of maxilla as long anteroposteriorly as tall; 33, lacrimal anterior ramus dorsoventrally narrow; 34, lacrimal foramen small, positioned at mid-height along ventral ramus; 35, postorbital ventral process with U-shaped cross section; 36, quadrate foramen reduced or absent; 37, radius less than 50% of humeral length; 38, manual digit I ungual elongate (three times the height of proximal articular end). **Allosauroidea** (plus unresolved subgroups): 39, nasal participation in antorbital fossa; 40, excavated internal carotid artery canal; 41, basiptyergoid processes very short; 42, quadrate with broad articular flange for quadratojugal; 43, palatine with flange-shaped process for lacrimal; 44, basioccipital excluded from the basal tubera; 45, articular with pendant medial process; 46, quadrate short, head near mid-orbit; 47, surangular twice maximum depth of angular (which equals a reduced external mandibular fenestra). **Carcharodontosauridae** (plus included node): 48, broad postorbital-lacrimal contact; 49, postorbital with suborbital flange; 50, dentary with squared, expanded anterior end; 51, pubic boot 30% of pubic length; 52, ventral extension of basisphenoid; 53, midcervical centra (posterior articular face) at least 20% broader than tall; 54, elevation of anterior face absent in midcervical centra; 55, rudimentary caudal pleurocoels. **Coelurosauria** (plus included node): 56, antorbital fossa anterior margin 40 to 50% of the anteroposterior width of fossa; 57, ectopterygoid pneumatic excavation subcircular; 58, caudal 15 and more posterior caudals with elongate prezygapophyses; 59, coracoid postroventral process length more than twice glenoid diameter; 60, ischial obturator flange triangular; 61, pubic obturator notch; 62, femoral fourth trochanter weak or absent; 63, fibular fossa occupying all of the medial aspect of the proximal end.
46. Supported by The David and Lucile Packard Foundation, the National Geographic Society, and The Eppley Foundation for Research. We thank C. Abrazcinskas for executing the finished illustrations; Q. Cao, R. Macek, and G. Wilson for fossil preparation; M.-S. Cornier, J. Hopson, A. Milhi, and H.-D. Sues for their contributions in the field; M. Carrano, J. Hopson, and H.-D. Sues for reviewing an earlier draft of the paper; and M. Bensaïd and M. Dahmani (Ministère de l'Energie et des Mines, Rabat, Morocco) for their support of this research.

29 February 1996; accepted 3 April 1996

## Lead and Helium Isotope Evidence from Oceanic Basalts for a Common Deep Source of Mantle Plumes

B. B. Hanan and D. W. Graham

Linear arrays in lead isotope space for mid-ocean ridge basalts (MORBs) converge on a single end-member component that has intermediate lead, strontium, and neodymium isotope ratios compared with the total database for oceanic island basalts (OIBs) and MORBs. The MORB data are consistent with the presence of a common mantle source region for OIBs that is sampled by mantle plumes.  $^3\text{He}/^4\text{He}$  ratios for MORBs show both positive and negative correlation with the  $^{206}\text{Pb}/^{204}\text{Pb}$  ratios, depending on the MORB suite. These data suggest that the common mantle source is located in the transition zone region. This region contains recycled, oceanic crustal protoliths that incorporated some continental lead before their subduction during the past 300 to 2000 million years.

Earth's mantle is geochemically heterogeneous, but the origin, scale, and distribution of chemical variations are uncertain. Analyses of oceanic basalt isotope compositions

seem to indicate mixtures of at least four mantle components (1). Recently, another mantle component located internal to these four was identified on the basis of Sr-Nd-Pb-He isotope data (2–4). Trends of Pb isotope data for MORB suites converge on a position internal to the global mantle components and define a common end-member for MORBs (5). Here, we show that the MORB and OIB data define the same inter-

B. B. Hanan, Department of Geological Sciences, San Diego State University, San Diego, CA 92182-1020, USA.

D. W. Graham, College of Oceanic and Atmospheric Sciences, Oregon State University, Corvallis, OR 97331-5503, USA.

nal component. By restricting our initial analysis to MORBs, we avoided complications from plume-lithosphere interactions. Trends in the MORB Pb and He data provide information on the origin and location (depth) of this common source reservoir (6).

There are about 900 Pb isotope analyses of MORBs (7). The Pb isotope data for Pacific, Indian, and Atlantic MORBs define distinct trends that converge to a common Pb isotopic value (Table 1). The statistics of the fit for the data for each region are considerably more significant than for the whole data set, supporting the notion of separating the data into subpopulations. MORBs are generally considered to derive from the large ion lithophile element-depleted asthenosphere. When the MORB data are filtered to exclude plume-related samples by using the criteria  $(La/Sm)_N \leq 0.75$  (the ratio normalized to chondrites), convergence of the three trends is still observed (5). The convergence shown by the three arrays is not an artifact of recent plume-ridge interactions.

The common Pb isotopic composition (8) at the point of convergence for the three MORB subpopulations lies in a position internal to the components DM (depleted mantle source for MORB), EM1 and EM2 (enriched mantle 1 and 2), and HIMU

(high-U/Pb mantle). The component common to all MORBs has  $^{206}Pb/^{204}Pb \approx 19.2$  to 19.8,  $^{207}Pb/^{204}Pb \approx 15.55$  to 15.65, and  $^{208}Pb/^{204}Pb \approx 38.8$  to 39.6; and for the same data,  $^{87}Sr/^{86}Sr \approx 0.703$  to 0.704 and  $\epsilon_{Nd} \approx 4$  to 6 (9) (Fig. 1). We refer to this common component as C. The three MORB arrays are distinguished by differences in the relative proportions of DM and EM1 components in the least radiogenic, binary-like end-member. The Indian Ocean MORBs define the most EM1-rich array, and the Pacific MORBs the least, with the Atlantic MORBs intermediate.

In the ternary Pb isotope diagram many OIB arrays display a radial pattern, sweeping from the HIMU pole through EM2-EM1-DM, with C at the center (Fig. 1B). Basalts from Pitcairn, Heard, Galápagos, and Easter Island define arrays pointing toward C that can be described as having different proportions of Pb from DM and EM1, suggesting that material with EM1 and DM compositions may have been intimately associated in some sources (10). The St. Helena, Guadalupe, and Sao Miguel arrays trend toward C and can be described as having fixed proportions of HIMU- and EM2-like Pb. The radial pattern converging at C suggests that different mantle materials were mixed systematically to produce the

basalts. During the most recent mixing event, material having C composition interacted with multicomponent mixtures, resulting in the pseudobinary trends observed in the OIBs. The multicomponent mixtures are inferred to have formed during an earlier mixing event involving the more extreme Pb isotope compositions (11).

High  $^3He/^4He$  ratios are a characteristic of OIBs lying between C and the DM-EM1 poles (Fig. 1B). Basalts that plot near the HIMU-EM2 multicomponent mixtures have relatively low  $^3He/^4He$ . Samoa is different and can be described as an EM2-EM1 mixture trend toward C with high  $^3He/^4He$  ratios. Because high  $^3He/^4He$  ratios are not a characteristic of DM, the high  $^3He/^4He$  reservoir must have C or EM1-like Pb. In general,  $^3He/^4He$  ratios increase in basalts trending toward C (for example, Samoa, Galápagos, and Pitcairn), consistent with the notion that the C reservoir has a high  $^3He/^4He$  ratio. However, in detail the relations between Pb and He isotopes for OIBs are more complicated. For example, on Hawaii individual shield volcanoes follow two curved geographic trends, the Loa and Kea trends. Tholeiitic basalts along the Loa trend have higher relative  $^{208}Pb$  and lower relative  $^{206}Pb$  than those along the Kea trend (12). The tholeiites generally represent the volcanic

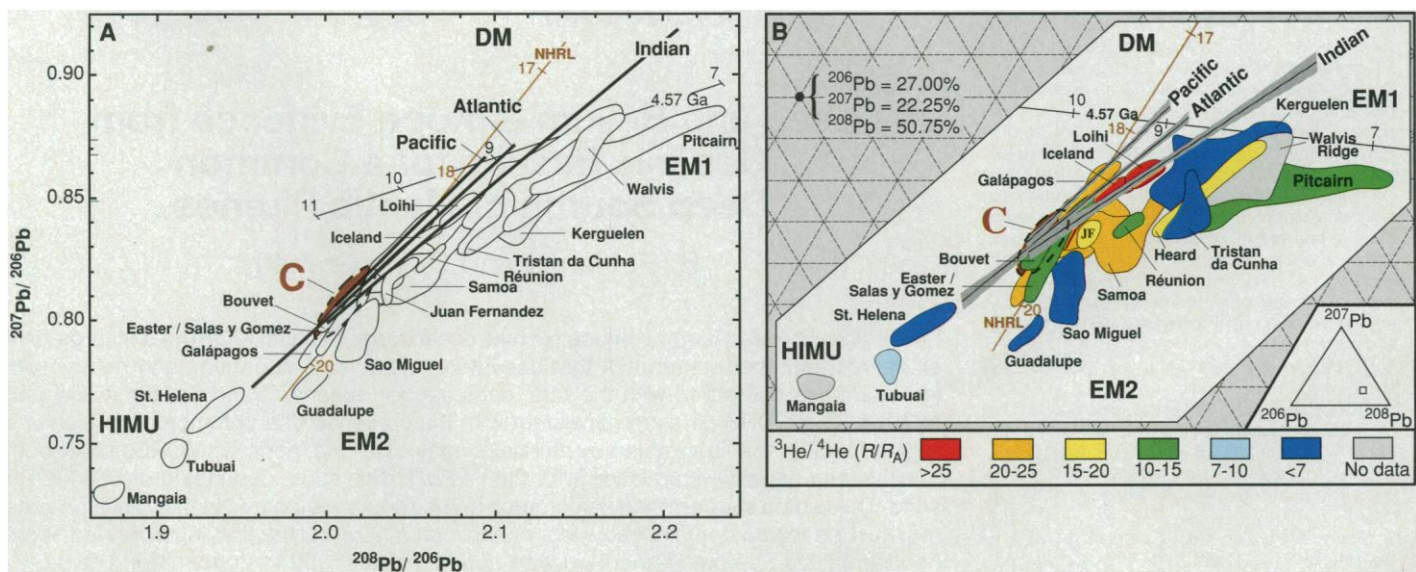


**Fig. 1.** (A)  $^{208}Pb/^{206}Pb$  versus  $^{207}Pb/^{206}Pb$  covariation diagram showing the converging regression lines for the three MORB subpopulations (Atlantic, Pacific, and Indian) in relation to the OIB fields and the global isotopic end-member components HIMU, EM1, EM2, and DM (1). The end-member components encompass the entire oceanic basalt database and plot in more extreme positions than the general positions shown in the diagrams. Lines and fields are based on published data (7). (B) Ternary plot of the relative abundances of  $^{206}Pb$ ,  $^{207}Pb$ , and  $^{208}Pb$  for the same data as shown in (A). The 95% confidence curves are shown for the converging regression lines of the three MORB subpopulations. The Northern Hemisphere reference line (NHRL) (36) and the 4.57-billion-year (Ga) geochron are shown for reference. Numbers in brown along the NHRL are corresponding values of  $\mu$  ( $^{238}U/^{204}Pb$ ), and numbers along the geochron are corresponding values of  $\mu$  ( $^{238}U/^{204}Pb$ ), with constant  $\kappa$  ( $^{232}Th/^{238}U$ ) = 4.2. The ternary grid spacing

is 0.25%. The topology of the  $^{208}Pb/^{206}Pb$  versus  $^{207}Pb/^{206}Pb$  covariation diagram and the ternary relative Pb isotope diagram are essentially identical, but the latter diagram allows better visualization of mixing relations than the binary Pb/Pb diagram. The OIB fields are color coded for the highest  $^3He/^4He$  ( $R/R_A$ ) ratios ( $R/R_A$  is the isotopic ratio expressed relative to the atmospheric  $^3He/^4He$  ratio of  $1.39 \times 10^{-6}$ ) for the OIB suites with published He isotope data (7). The highest terrestrial volcanic  $^3He/^4He$  ratios are found at the Hawaiian and Iceland hot spots. The relative Pb isotope fields for Iceland neovolcanics and Loihi tholeiites are shown; other Hawaiian volcanoes are omitted for clarity. The OIB arrays converge in an intermediate position relative to DM, EM1, EM2, and HIMU and help to constrain the composition of the internal component. The Tertiary Iceland volcanics (not shown on this diagram) also trend toward the internal component from the DM-EM1 region of the diagram (37).

stage during which the plume material is most easily recognized (13). The Pb isotope data for Loa and Kea tholeiites from Hawaii and for tholeiites from Loihi seamount define two distinct geographic trends that point toward C. These patterns suggest that the lavas are derived from mantle representing mixtures of C and a heterogeneous source having less radiogenic Pb that comprises different proportions of DM- and EM1-like material. In general, the  $^3\text{He}/^4\text{He}$  ratios increase in lavas plotting toward C, but higher  $^3\text{He}/^4\text{He}$  ratios are also associated with the more EM1-rich Loa trend. Similar complexity is shown by the MORB data.

In Pacific MORBs the  $^3\text{He}/^4\text{He}$  ratios are high in basalts with Pb isotopic values close to C.  $^3\text{He}/^4\text{He}$  ratios increase with  $^{206}\text{Pb}/^{204}\text{Pb}$  ratios for Pacific MORBs from the Easter Microplate (14) and near 17°S on the East Pacific Rise (15) (Fig. 2). However, in the Atlantic, at 14°N (16) and 33°S (17), the case is reversed;  $^3\text{He}/^4\text{He}$  ratios decrease with increasing  $^{206}\text{Pb}/^{204}\text{Pb}$  ratios (Fig. 2). Furthermore, within the Atlantic and Indian Ocean MORB data there is also a hint of higher  $^3\text{He}/^4\text{He}$  ratios in basalts that lie closer to EM1. In detail, Atlantic MORB data in Fig. 1B resemble a fanlike pattern radiating from C where the  $^3\text{He}/^4\text{He}$  ratio appears to increase as the proportion of EM1 increases at the expense of DM. Similarly, the two highest  $^3\text{He}/^4\text{He}$  ratios for Indian Ocean MORBs are from basalt glasses with higher proportions of EM1.

These Pb-He isotope observations from both MORBs and OIBs raise the possibility that what is collectively referred to as EM1 may actually represent two mantle reservoirs, both with long-term enrichment in U/Pb and Th/Pb relative to DM. Perhaps one reservoir represents recycled crustal material with low  $^3\text{He}/^4\text{He}$ , and the other,

relatively primitive mantle material with high  $^3\text{He}/^4\text{He}$ .

Hart *et al.* (2) observed that the OIB data plot within a tetrahedron in  $^{87}\text{Sr}/^{86}\text{Sr}$ - $^{143}\text{Nd}/^{144}\text{Nd}$ - $^{206}\text{Pb}/^{204}\text{Pb}$  space with apices corresponding to the global mantle components EM1, EM2, HIMU, and DM, and that most arrays converge on a volume near the tetrahedron's base, which they termed the "focal zone" (FOZO). They also suggested that FOZO may be the high  $^3\text{He}/^4\text{He}$  mantle reservoir (2). Because FOZO is common to many hot spot mantle sources, Hart and co-workers (2, 3) reasoned that it represents the composition of the lower mantle entrained by plumes rising from the core-mantle boundary. Farley *et al.* (4) also described a component common to plumes that has high  $^3\text{He}/^4\text{He}$  ratios, called the primitive helium mantle (PHEM). In general, high  $^3\text{He}/^4\text{He}$  ratios in OIBs are associated with intermediate Nd, Sr, and Pb isotope ratios relative to the global mantle end-members (18). These observations collectively suggest a component common to many plumes that has intermediate Pb, Sr, and Nd isotope ratios and sometimes high  $^3\text{He}/^4\text{He}$  ratios. The common components FOZO and PHEM, defined on the basis of the OIB data, and C, defined solely on the basis of MORB isotope variations, have roughly similar Pb, Nd, and Sr isotope characteristics and may therefore represent the same mantle reservoir (19).

Carbon cannot represent an extremely old reservoir, because it is too rich in  $^{206}\text{Pb}$  relative to  $^{207}\text{Pb}$ , and it plots far below the 4.57-Ga geochron for the bulk Earth (Fig. 3) (20). It is therefore unlikely that C represents a major part of the mantle such as the lower mantle, because the total continental crust and the depleted mantle also plot below the 4.57-Ga geochron (21), and

mass balance would require an unidentified reservoir above the geochron. If the start of terrestrial Pb isotope evolution is significantly younger than 4.57 Ga—for example, 4.46 Ga (22)—then we cannot rule out the possibility that C represents the lower mantle on the basis of the Pb isotopes alone. The observation that Ce/Pb ratios in both OIBs and MORBs are uniform at  $25 \pm 5$  and significantly higher than both crustal (Ce/Pb = 4) and primitive mantle (Ce/Pb = 11) values (23) presents a serious mass balance problem if C represents the composition of the entire lower mantle, and we therefore consider this unlikely.

Mantle containing subducted oceanic crust (24) adequately accounts for C. Recycled oceanic crust, with an age of 300 to 2000 million years ago (Ma), is a viable source that satisfies the Pb isotope constraints (Fig. 3). For example, the Pb isotope composition of C can be obtained from 300-million-year-old oceanic crust with a  $^{238}\text{U}/^{204}\text{Pb}$  ( $\mu$ ) = 30 and  $^{232}\text{Th}/^{238}\text{U}$  ( $\kappa$ ) = 2 to 3, provided that some continental crustal Pb was incorporated before subduction.

The C reservoir must be located deeper in the mantle than the upper mantle MORB source because lava suites radiate from C. It follows that other components are mixed before there is mixing with material having the composition of C. A physical model consistent with this chronology would place C in the lower mantle, perhaps at the core-mantle boundary where plumes are thought to originate, or alternatively at the 670-km boundary layer between the upper and lower mantle. The other components are therefore located higher in Earth's mantle above the C

**Table 1.** Least squares linear regression parameters for MORBs. The ratios listed for the Pb/Pb diagram refer to the following covariation diagrams:  $^{207}\text{Pb}/^{206}\text{Pb} = ^{206}\text{Pb}/^{204}\text{Pb}$  versus  $^{207}\text{Pb}/^{204}\text{Pb}$ ;  $^{208}\text{Pb}/^{206}\text{Pb} = ^{206}\text{Pb}/^{204}\text{Pb}$  versus  $^{208}\text{Pb}/^{204}\text{Pb}$ ; and  $^{207}\text{Pb}/^{208}\text{Pb} = ^{208}\text{Pb}/^{206}\text{Pb}$  versus  $^{207}\text{Pb}/^{206}\text{Pb}$ .

Pb/Pb diagram	Slope	Intercept
	<i>All MORBs combined (n = 866)</i>	
$^{207}\text{Pb}/^{206}\text{Pb}$	$0.08764 \pm 0.00211$	$13.890 \pm 0.039$
$^{208}\text{Pb}/^{206}\text{Pb}$	$0.89652 \pm 0.01538$	$21.541 \pm 0.284$
$^{207}\text{Pb}/^{208}\text{Pb}$	$0.56555 \pm 0.00656$	$-0.32692 \pm 0.01353$
	<i>Atlantic MORB (n = 390)</i>	
$^{207}\text{Pb}/^{206}\text{Pb}$	$0.09228 \pm 0.00277$	$13.805 \pm 0.052$
$^{208}\text{Pb}/^{206}\text{Pb}$	$0.98388 \pm 0.01542$	$19.902 \pm 0.287$
$^{207}\text{Pb}/^{208}\text{Pb}$	$0.64565 \pm 0.00875$	$-0.49167 \pm 0.01796$
	<i>Pacific MORB (n = 267)</i>	
$^{207}\text{Pb}/^{206}\text{Pb}$	$0.12659 \pm 0.00440$	$13.159 \pm 0.081$
$^{208}\text{Pb}/^{206}\text{Pb}$	$1.11465 \pm 0.02085$	$17.359 \pm 0.385$
$^{207}\text{Pb}/^{208}\text{Pb}$	$0.68297 \pm 0.01278$	$-0.56404 \pm 0.02628$
	<i>Indian MORB (n = 209)</i>	
$^{207}\text{Pb}/^{206}\text{Pb}$	$0.07542 \pm 0.00473$	$14.126 \pm 0.086$
$^{208}\text{Pb}/^{206}\text{Pb}$	$0.87407 \pm 0.03062$	$22.171 \pm 0.558$
$^{207}\text{Pb}/^{208}\text{Pb}$	$0.57344 \pm 0.01223$	$-0.34821 \pm 0.02559$

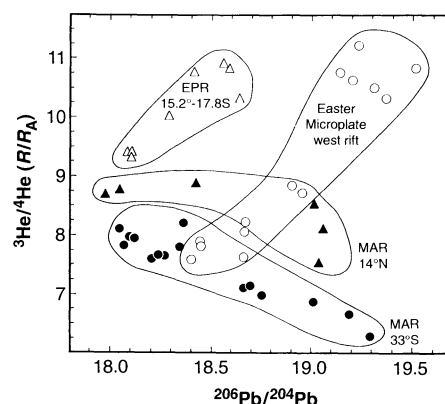


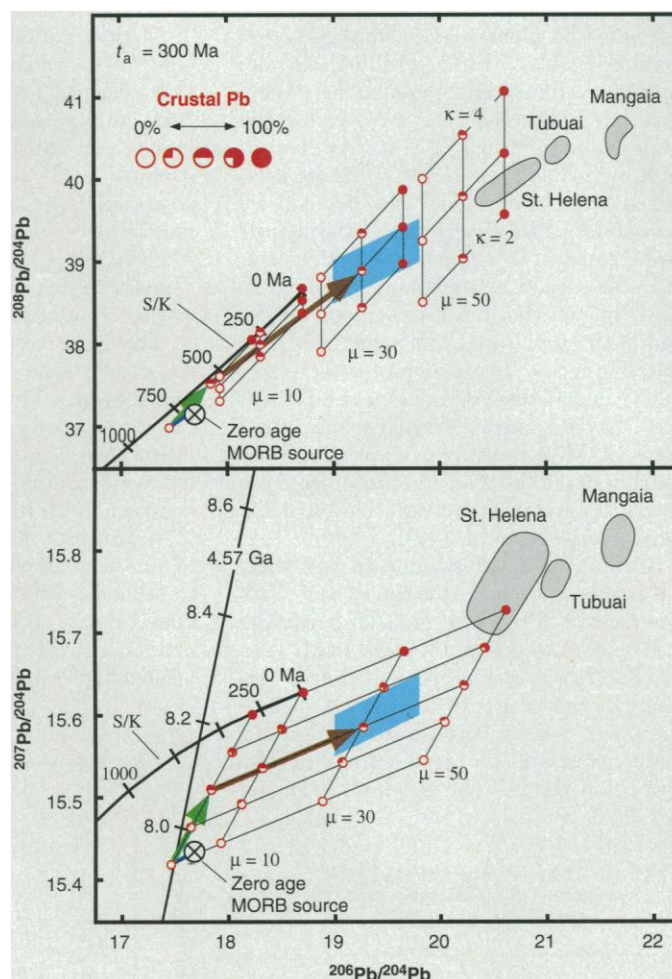
**Fig. 2.**  $^3\text{He}/^4\text{He}$  and  $^{206}\text{Pb}/^{204}\text{Pb}$  covariation diagram for Pacific and Atlantic ridge segments (14–17). Note that the  $^3\text{He}/^4\text{He}$  ratio is positively correlated with the  $^{206}\text{Pb}/^{204}\text{Pb}$  ratio for Pacific MORBs from the west rift of the Easter Microplate and near 17°S on the East Pacific Rise (EPR) where the Pb isotope arrays point toward C. For ridge segments on the Mid-Atlantic Ridge (MAR) near 14°N and 33°S, the trend is reversed and  $^3\text{He}/^4\text{He}$  is negatively correlated with  $^{206}\text{Pb}/^{204}\text{Pb}$  as the proportion of C increases.

reservoir. They are entrained as a plume rises and mix with each other before mixing with a plume core that is composed of C material (25). The observation that C can have both lower and higher  $^3\text{He}/^4\text{He}$  ratios than normal MORB suggests an origin from a thermal boundary layer, below which the high  $^3\text{He}/^4\text{He}$  reservoir is located. However, the precise location of the C reservoir is difficult to constrain from this observation alone. Because the lower mantle is usually considered to be a high  $^3\text{He}/^4\text{He}$  reservoir (26), C may represent the average composition of the

transition zone above the 670-km seismic discontinuity, which separates the upper and lower mantle. Carbon material with low  $^3\text{He}/^4\text{He}$  ratios may originate from regions of the transition where recycled or altered oceanic crust has been stored (27). The entrainment of small plumes or diapirs of such material from the upper parts of the transition zone into the overlying convection scheme may account for the negative correlations of  $^{206}\text{Pb}/^{204}\text{Pb}$  and  $^3\text{He}/^4\text{He}$  in some areas, such as at  $14^\circ\text{N}$  and  $33^\circ\text{S}$  on the Mid-Atlantic Ridge (16, 17). The occurrence of C mate-

rial with high  $^3\text{He}/^4\text{He}$  ratios may be due to a relatively larger amount of mass transfer from the lower mantle and would account for positive correlations between  $^{206}\text{Pb}/^{204}\text{Pb}$  and  $^3\text{He}/^4\text{He}$  such as is observed in MORBs from the Easter Microplate and near  $17^\circ\text{S}$  on the East Pacific Rise (14, 15). Episodes of high mass transfer may correlate with mantle overturn between the mesosphere and core-mantle boundary layers (28). The regional distribution of recycled crust at the base of the upper mantle may account for some of the contrasts in Pb-He isotope covariations for MORBs.

**Fig. 3.**  $^{207}\text{Pb}/^{206}\text{Pb}$  and  $^{208}\text{Pb}/^{206}\text{Pb}$  covariation diagrams illustrating possible models for the origin of the Pb isotope composition of C (light blue box), by hydrothermal alteration (green arrows) and subsequent aging (brown arrows) and recycling of oceanic crust. Grids illustrate the fraction of Pb exchanged during hydrothermal alteration 300 million years ago (Ma) ( $t_a$ ), between the mid-ocean ridge crust and continental crust or sediment having Stacey-Kramers Pb isotope composition (38). The thick, black, curved line represents the evolution of Stacey-Kramers Pb; tick marks [intervals of 250 million years (My)] show its Pb isotope composition in the past. The 4.57-Ga geochron is shown for reference; tick marks correspond to  $\mu$  values. The initial Pb isotope composition of the unaltered mid-ocean ridge crust has been backtracked from the end-member Atlantic-Pacific Pb isotope compositions (dark blue line, lower left) given by Al-*l*egre *et al.* (22), assuming a depleted mantle with  $\mu = 5$  and  $\kappa = 2.5$  [see (39)]. The proportion of continental Pb incorporated at that point in time specifies the initial Pb isotope composition at the end of hydrothermal alteration before subduction. The green and brown arrows track the evolutionary trajectory for the specific case of 50% exchange where  $\mu = 30$  and  $\kappa = 3$  for  $t_a = 300$  My. This process may involve mediation by metalliferous sediments and hydrothermal sulfide deposits (40). In the  $^{208}\text{Pb}/^{206}\text{Pb}$  covariation diagram, the vertical grid lines denote the Pb isotope compositions resulting from closed-system radioactive decay for the specified  $\mu$  and the initial Pb isotope compositions produced during the hydrothermal alteration; the steep grid lines correspond to constant values for the ratio of MORB to continental Pb and for  $\kappa$ . In the  $^{207}\text{Pb}/^{206}\text{Pb}$  covariation diagram, the steep grid lines correspond to constant values of  $\mu$  with varying proportions of MORB to continental Pb; the less steep lines correspond to constant proportions of MORB to continental Pb with varying values of  $\mu$ . The Pb isotope compositional range of C suggests an origin from altered oceanic crustal protoliths that have incorporated continental Pb before subduction and were recycled during the past 300 to 2000 My. Also note that the  $^{207}\text{Pb}/^{206}\text{Pb}$  and  $^{208}\text{Pb}/^{206}\text{Pb}$  slopes of the St. Helena HIMU-like array are similar to the model grids. If we took a more radiogenic crustal Pb relative to Stacey-Kramers Pb, such as that for modern pelagic sediments (41), St. Helena-like Pb isotope compositions would be produced from a variably polluted, altered oceanic crust in several hundred million years, unlike the 1 to 2 billion years often cited.



## REFERENCES AND NOTES

1. W. M. White, *Geology* **13**, 115 (1985); C. J. Allègre, B. Hamelin, A. Provost, B. Dupré, *Earth Planet. Sci. Lett.* **81**, 319 (1986); A. Zindler and S. R. Hart, *Annu. Rev. Earth Planet. Sci.* **14**, 493 (1986).
2. S. R. Hart, E. H. Hauri, L. A. Oschmann, J. A. Whitehead, *Science* **256**, 517 (1992).
3. E. H. Hauri, J. A. Whitehead, S. R. Hart, *J. Geophys. Res.* **99**, 24275 (1994).
4. K. A. Farley, J. H. Natland, H. Craig, *Earth Planet. Sci. Lett.* **111**, 183 (1992).
5. B. B. Hanan, paper presented at the Mantle Plume Symposium, California Institute of Technology, Pasadena, CA, 1 to 3 May 1991; \_\_\_\_\_ and D. W. Graham, *Eos* **75** (no. 16), 67 (1994); *XXI General Assembly, IUGG*, Boulder, CO, July 1995 (International Union of Geodesy and Geophysics, Toulouse, France, 1995), p. B418.
6. B. B. Hanan, R. H. Kingsley, J.-G. Schilling, *Nature* **322**, 137 (1986); D. W. Graham *et al.*, *Earth Planet. Sci. Lett.* **110**, 133 (1992). For example, variations in Pb and He isotopes for South Atlantic MORBs show that heterogeneities in the upper mantle MORB source beneath this region are highly structured and dominated by distinct east-west channels connecting the off-ridge plumes and the westward migrating ridge. The heterogeneities are expressed as anomalous spike-like dispersions in the Pb and He isotope ratios at the latitudes of the off-ridge hot spot islands. These preferential flows are superimposed on a previous broad radial dispersion of the off-ridge plume material into the asthenosphere before the opening of the South Atlantic and juxtaposition of the ridge and plumes. This prior mixing event is expressed by the broad background variation of the normal MORBs between the anomalous spikes; the more recent hot spot-ridge mixing event is recorded by distinct Pb isotope arrays between the off-ridge hot spots and the mantle beneath the ridge opposite the hot spots.
7. We used published analyses and our unpublished Pb and He isotope data. References for the MORB and OIB isotope database are available from the authors on request.
8. Pb isotope data are commonly displayed by diagrams that allow the relative variations in the three radiogenic Pb isotope tracers  $^{206}\text{Pb}$ ,  $^{207}\text{Pb}$ , and  $^{208}\text{Pb}$  to be viewed simultaneously. The simplest method is a binary Pb/Pb diagram of  $^{208}\text{Pb}/^{206}\text{Pb}$  versus  $^{207}\text{Pb}/^{206}\text{Pb}$  (Fig. 1A). Two other methods are to plot the three Pb isotope ratios  $^{206}\text{Pb}/^{204}\text{Pb}$ ,  $^{207}\text{Pb}/^{204}\text{Pb}$ , and  $^{208}\text{Pb}/^{204}\text{Pb}$  on mutually perpendicular axes (1) or to plot the three ratios in the triangular relative  $^{206}\text{Pb}$ - $^{207}\text{Pb}$ - $^{208}\text{Pb}$  diagram (5). In the triangular diagram, only one projection is required to view the entire topology, and it allows better visualization of mixing relations than the binary Pb/Pb diagram. However, the triangular diagram is a simplex rather than a vector space so quantitative modeling of multicomponent mixing is more limited.
9. The value for  $\epsilon_{\text{Nd}}$  is
 
$$\left( \frac{^{143}\text{Nd}/^{144}\text{Nd}_{\text{measured}}}{^{143}\text{Nd}/^{144}\text{Nd}_{\text{CHUR}}} - 1 \right) \times 10^4$$

where  $^{143}\text{Nd}/^{144}\text{Nd}_{\text{CHUR}}$  is the value for a chondritic uniform reservoir at present [D. H. DePaolo and G. J.

Wasserburg, *Geophys. Res. Lett.* **3**, 249 (1976).

10. This does not mean that these trends originate through the mixing of only two components. We believe that the linear trends record binary-like mixing between a volume of mantle with composition C and another mantle volume of distinct isotope composition that can be described by reference to the external components. We use the notion of mantle components as reference coordinates in isotope space. The isotopic composition of any particular volume of mantle is actually the product of a unique sequence of geological processes, not simply the mixing of the DM, EM, and HIMU components.

11. The MORB and OIB databases clearly show the tendency for oceanic basalt data to focus on the internal component C (2–4). However, not all individual OIB and MORB data suites converge on C. For example, in the equatorial Atlantic, local mixing vectors in Pb/Pb isotope space extend beyond C with  $^{206}\text{Pb}/^{204}\text{Pb} > 20$  as a result of hot spot–ridge interaction between the MORB mantle beneath the ridge at 1.7°N and the Sierra Leone plume (29). The Sierra Leone plume can be viewed as a multicomponent mixture of C-like, HIMU-like, and local depleted mantle. Other examples of hot spot–ridge interactions that show similar complexity include the Reykjanes Ridge (30), the southern Mid-Atlantic Ridge (5), and Galápagos spreading center (31). We view plumes as consisting of both C material and other materials of variable compositions that can be described as multicomponent mixtures of the external components DM, EM1, EM2, and HIMU, with a multistage history of mixing (10).

12. M. Tatsumoto, *Earth Planet. Sci. Lett.* **38**, 63 (1978).

13. M. D. Feigenson, *J. Geophys. Res.* **91**, 9383 (1986); M. Tatsumoto, E. Hegner, D. M. Unruh, *U.S. Geol. Surv. Prof. Paper 1350* (1987), p. 723; M. D. Kurz, W. J. Jenkins, S. R. Hart, D. Clague, *Earth Planet. Sci. Lett.* **66**, 388 (1983); M. D. Kurz, M. O. Garcia, F. A. Frey, P. A. O'Brien, *Geochim. Cosmochim. Acta* **51**, 2905 (1987); H. Staudigel *et al.*, *Earth Planet. Sci. Lett.* **69**, 13 (1984); C. Y. Chen and F. A. Frey, *Nature* **302**, 785 (1983); M. O. Garcia, D. W. Muenow, K. E. Aggrey, J. R. O'Neil, *J. Geophys. Res.* **94**, 10525 (1989).

14. B. B. Hanan and J.-G. Schilling, *J. Geophys. Res.* **94**, 7432 (1989); R. J. Poreda, J.-G. Schilling, H. Craig, *Earth Planet. Sci. Lett.* **119**, 319 (1993).

15. J. J. Mahoney *et al.*, *Earth Planet. Sci. Lett.* **121**, 173 (1993).

16. L. Dosso, B. B. Hanan, H. Bougault, J.-G. Schilling, J.-L. Joron, *ibid.* **106**, 29 (1991); T. Staudacher *et al.*, *ibid.* **96**, 119 (1989).

17. B. B. Hanan, D. W. Graham, P. J. Michael, J.-G. Schilling, *Eos* **73**, 582 (1992); B. B. Hanan, D. W. Graham, P. J. Michael, *Min. Mag.* **58A**, 370 (1994).

18. D. W. Graham, D. M. Christie, K. S. Harpp, J. E. Lupton, *Science* **262**, 2023 (1993).

19. C and PHEM have similar intermediate  $^{87}\text{Sr}/^{86}\text{Sr}$  and  $^{143}\text{Nd}/^{144}\text{Nd}$  ratios, approximately 0.7035 versus 0.7047 and 0.51290 versus 0.51273 [ $\epsilon_{\text{Nd}}$  (9) of 5.0 versus 1.8], respectively (4, 5). In contrast, FOZO originally was estimated to have depleted  $^{87}\text{Sr}/^{86}\text{Sr}$  ratios and  $^{143}\text{Nd}/^{144}\text{Nd}$  isotope signatures of about 0.7025 and 0.51314 ( $\epsilon_{\text{Nd}} = 10$ ), respectively (2), but these have been modified to  $^{87}\text{Sr}/^{86}\text{Sr} = 0.7035$  and  $^{143}\text{Nd}/^{144}\text{Nd} = 0.5129$  (3).

20. We use the 4.57-Ga reference geochron determined from meteorites (32) as a reference to discuss the Pb isotope composition for the bulk Earth and mass balance for Earth's Pb reservoirs in the  $^{206}\text{Pb}/^{204}\text{Pb}$  versus  $^{207}\text{Pb}/^{204}\text{Pb}$  diagram. Meteorites and Earth are assumed to have a common age and to have initially had the same Pb isotope composition because meteorites and average modern terrestrial Pb fall on the same Pb/Pb isochron, the 4.57-Ga geochron. This geochron is the locus of all Earth reservoirs that have evolved from Earth's starting Pb isotope composition, but with different U/Pb ratios. Because most mantle and crustal rocks plot below the geochron and because the bulk Earth must lie on it, either an unknown reservoir plotting above the 4.57-Ga geochron or a younger age for Earth's Pb, moving the geochron down, is required to achieve mass balance.

21. R. L. Rudnick and S. L. Goldstein, *Earth Planet. Sci. Lett.* **98**, 192 (1990).

22. C. J. Allègre, E. Lewin, B. Dupré, *Chem. Geol.* **70**,

211 (1988); S. J. G. Galer and S. L. Goldstein, *Geophys. Monogr. Am. Geophys. Union*, in press; G. Manhès, C. J. Allègre, B. Dupré, B. Hamelin, *Earth Planet. Sci. Lett.* **44**, 91 (1979).

23. A. W. Hofmann, K. P. Jochum, M. Seufert, W. M. White, *Earth Planet. Sci. Lett.* **79**, 33 (1986).

24. A. W. Hofmann and W. M. White, *ibid.* **57**, 421 (1982); M. T. McCulloch, *ibid.* **115**, 89 (1993).

25. The external components EM1, EM2, and HIMU are generally thought to represent recycled materials that may accumulate in regions of phase transition or density contrast (33, 34). Likely locations include the core-mantle boundary, the upper-lower mantle transition, or the shallowest asthenosphere (perisphere) (35). The regional distribution of these materials within the mantle may account for some of the contrasts in the Pb and He isotope covariations for the MORB subpopulations.

26. C. J. Allègre, T. Staudacher, P. Sarda, M. Kurz, *Nature* **303**, 762 (1983); R. K. O'Nions and E. R. Oxburgh, *ibid.* **306**, 429 (1983); L. H. Kellogg and G. J. Wasserburg, *Earth Planet. Sci. Lett.* **99**, 276 (1990).

27. A. E. Ringwood, S. E. Kesson, W. Hibberson, N. Ware, *Earth Planet. Sci. Lett.* **113**, 521 (1992).

28. P. J. Tackley, D. J. Stevenson, G. A. Glatzmaier, G. Schubert, *Nature* **361**, 699 (1993); M. Stein and A. W. Hofmann, *ibid.* **372**, 63 (1994).

29. J.-G. Schilling, B. B. Hanan, B. McCully, R. H. Kingsley, D. Fontignie, *J. Geophys. Res.* **99**, 12005 (1994).

30. C. H. Langmuir, R. D. J. Vocke, G. N. Hanson, S. R. Hart, *Earth Planet. Sci. Lett.* **37**, 380 (1978); S.-S. Sun, M. Tatsumoto, J.-G. Schilling, *Science* **190**, 143 (1975).

31. S. P. Verma and J.-G. Schilling, *J. Geophys. Res.* **87**,

10838 (1982); S. P. Verma, J.-G. Schilling, D. G. Wagoner, *Nature* **306**, 654 (1983).

32. C. Patterson, *Geochim. Cosmochim. Acta* **10**, 230 (1956).

33. C. G. Chase, *Earth Planet. Sci. Lett.* **52**, 277 (1981); M. T. McCulloch, *ibid.* **115**, 89 (1993).

34. C. J. Allègre and D. L. Turcotte, *Geophys. Res. Lett.* **12**, 207 (1985); D. McKenzie and R. K. O'Nions, *Nature* **301**, 229 (1983); A. E. Ringwood, *J. Geol.* **90**, 611 (1982).

35. D. L. Anderson, *Rev. Geophys.* **33**, 125 (1995).

36. S. R. Hart, *Nature* **309**, 753 (1984).

37. B. B. Hanan and J.-G. Schilling, *Geol. Soc. Aust. Abstr. Ser.* **27**, 43 (1991).

38. J. S. Stacey and J. D. Kramers, *Earth Planet. Sci. Lett.* **26**, 207 (1975).

39. W. M. White, *ibid.* **115**, 211 (1993).

40. D. M. Miller, S. L. Goldstein, C. H. Langmuir, *Nature* **368**, 514 (1994); B. Peucker-Ehrenbrink, A. W. Hofmann, S. R. Hart, *Earth Planet. Sci. Lett.* **125**, 129 (1994).

41. C. Patterson and M. Tatsumoto, *Geochim. Cosmochim. Acta* **28**, 1 (1964); S.-S. Sun, *Philos. Trans. R. Soc. London A* **297**, 409 (1980); D. Ben Othman, W. M. White, P. J. Patchett, *Earth Planet. Sci. Lett.* **94**, 1 (1989).

42. We are grateful for the perspectives and arguments expressed by D. Anderson, K. Farley, S. Galer, R. Kingsley, J. Lupton, J.-G. Schilling, G. Wagoner, and W. White. Financial support was provided by the NSF.

10 October 1995; accepted 7 March 1996

## Pre–Main-Sequence Star Candidates in the Bar of the Large Magellanic Cloud

J. P. Beaulieu,\* H. J. G. L. M. Lamers, P. Grison, R. Julien, C. Lanciaux, R. Ferlet, A. Vidal-Madjar, E. Bertin, E. Maurice, L. Prévot, C. Gry, J. Guibert, O. Moreau, F. Tajhmady, E. Aubourg, P. Bareyre, J. de Kat, M. Gros, B. Laurent, M. Lachièze-Rey, E. Lesquoy, C. Magneville, A. Milsztajn, L. Moscoso, F. Queinnec, C. Renault, J. Rich, M. Spiro, L. Vigroux, S. Zylberajch, R. Ansari, F. Cavalier, M. Moniez

Candidate pre–main-sequence stars were observed in the bar of the Large Magellanic Cloud during the search for dark matter in the galactic halo. Seven blue stars of apparent visual magnitude 15 to 17 had irregular photometric variations and hydrogen emission lines in their optical spectra, which suggested that these stars are pre–main-sequence stars of about 10 solar masses. These stars are slightly more massive and definitely more luminous than are Herbig AeBe pre–main-sequence stars in our own galaxy. Continued observations of these very young stars from another galaxy, which are probably at the pre–hydrogen-burning stage, should provide important clues about early stages of star formation.

The early stages of star formation are generally hidden from optical observations because the stars are embedded in their circumstellar dust clouds. The lower the mass of a star, the slower its contraction toward the main sequence where H is ignited. Therefore, the only pre–main-sequence stars that are optically visible in the galaxy are the low-mass T Tauri stars ( $M \approx 1$  to  $5 M_{\odot}$ , where  $M_{\odot}$  is solar mass) and the slightly more massive Herbig AeBe (HAeBe) stars of 2 to  $9 M_{\odot}$ . In galaxies with a lower metallicity, the pre–main-sequence stars are expected to have less dust. This attribute might enable us to observe and study the pre–main-

sequence phase of more massive stars in other galaxies, thereby extending our knowledge of the early evolution of stars to younger phases. Here, we report the serendipitous discovery of HAeBe stars in the Large Magellanic Cloud (LMC) with the EROS experiment (1).

The EROS database was used to search for quasi-stellar objects (QSOs) behind the LMC for spectroscopic studies of the absorption components of gas in the LMC. About 10 to 12 QSOs down to magnitude  $\sim 20$  were expected in the field of the EROS charge-coupled device (CCD) camera. Because the EROS photometry has only two filters and it